Composites Part B 174 (2019) 106988

Contents lists available at ScienceDirect

Composites Part B

journal homepage: www.elsevier.com/locate/compositesb

Developing high performance PA 11/cellulose nanocomposites for industrial-scale melt processing

Priya Venkatraman [a], Anne M. Gohn [b], Alicyn M. Rhoades [b], E. Johan Foster [a,*]

[a] Department of Materials Science and Engineering, Macromolecules Innovation Institute, Virginia Tech, Blacksburg, VA, 24061, United States
[b] School of Engineering, PennState Behrend, 4701 College Drive, Erie, PA, 16563, United States

ARTICLE INFO

Keywords:
Polyamides
Cellulose nanocrystals
Processing
Nanocomposites
Crystallization kinetics

ABSTRACT

This study presents methods of developing thermally stable polyamide 11 (PA 11), cellulose nanocrystal (CNCs) composites able to withstand high temperature processing for high performance applications. Thus far, it has been difficult to use cellulose-based composites in industrial applications due to the high temperatures at which the materials would need to be processed. Sulfated CNCs (S–CNCs), the most commercially available CNCs, perform the poorest with respect to being thermally stable at high temperatures. Direct mixing techniques typically used to make these nanocomposites at a lab-scale, even at low concentrations of CNCs, have resulted in poor dispersion and thermal stability of CNCs. However, this paper offers industrially viable methods of fabricating composites that shield these S–CNCs from excessive thermal degradation during processing. We set out to determine the effect of pre-mixing CNCs and the polymer to obtain homogeneous and thermally stable nanocomposites for high temperature processing methods such as compression molding and injection molding. For the PA 11/CNC composites, fabrication through both milling and compounding resulted in reinforcement of the polymer with increased storage modulus in the rubbery plateau, and increased Young's modulus while preserving the toughness of PA 11. Furthermore, the milled samples showed higher stiffness than the compounded samples and surface charge density of the CNCs played a great role in the mechanical properties of the composites as it directly correlates with how well dispersed the composites were. Overall, this work shows the potential of pre-mixing methods to obtain high performance nanocellulose based composites through industrial manufacturing processes.

1. Introduction

Over the years, polyamide 11 (PA 11) has garnered a lot of interest for its potential use in a plethora of applications ranging from deep sea oil production, to lightweight replacements for metals and rubbers in automobiles and aircrafts, to high performance athletic shoes. PA 11 is a semi-crystalline polymer derived from castor oil, making it an excellent candidate as a bio-renewable material for composite applications. Due to production of PA 11 generating low CO_2 emission and it being entirely renewable, it has a smaller impact on climate change than its petroleum-based nylon counterparts and other conventional polymers. Furthermore, in addition to its mechanical performance, PA 11 boasts low specific gravity (~1.03 g cm^{-3}), excellent chemical, impact, and abrasion resistance, high thermal stability (T_m = ~180–190 °C), and has a wide range of processing temperatures ranging from 130 to 240 °C, making it easily processable [1].

To further increase the performance of PA 11 beyond its neat properties, fibrous or crystalline additives may be used to reinforce the polymer matrix. Reinforcing PA 11 with fillers is a cost-effective way to develop new polymeric composites with diverse and desired properties suitable for the aviation industry. When compared to synthetic fiber additives like glass, carbon, and Kevlar®, natural fibers exhibit a comparably lower density and can provide reinforcement capable of imparting high specific mechanical properties in advanced applications [2–4]. Industrial interest in polymer nanocomposites is driven by the fact that the incorporation of mechanically robust, high aspect ratio, nanoscale fillers can significantly enhance the mechanical properties in comparison to those of the neat polymer.

The incorporation of cellulose nanocrystals (CNCs) as a reinforcing agent in both thermoset and thermoplastic polymers has gained increasing appeal across a range of applications in many areas of engineering and technology. With cellulose being one of the most abundant

* Corresponding author.
E-mail address: johanf@vt.edu (E.J. Foster).

https://doi.org/10.1016/j.compositesb.2019.106988
Received 28 March 2019; Received in revised form 21 May 2019; Accepted 27 May 2019
Available online 30 May 2019

natural polymers, use of it as a reinforcement agent in PA 11 allows us to address challenges relating to biodegradability, energy, and cost. The remarkable mechanical properties of CNCs make them a suitable candidate for developing reinforced polymer composites. CNCs have a Young's modulus higher than that of glass fibers, around 70 GPa, which is similar to the properties of Kevlar [2]. Furthermore, these highly crystalline nanoparticles have a high aspect ratio due to their rod-like structure. These mechanical properties in addition to their environmentally friendly and renewable classification make them an appealing choice of additives for polymer nanocomposites [5,6]. However, there are several obstacles when it comes to using CNCs as a reinforcement agent in polymers [6]. One main obstacle is obtaining a homogeneous dispersion of CNCs within a continuous polymer matrix. However, this can be tackled by functionalizing the CNCs to alter surface charges causing a repulsion in the CNC–CNC interactions and driving the CNC-polymer interaction [7]. Sulfonation is one such method, and sulfated-CNCs is often the commercially available form of CNCs. However, this results in lowering the overall thermal stability of the CNCs [2,7–10]. This is the second main obstacle when it comes to utilizing CNCs as a reinforcement agent in polymers. Since most industrial polymer processing methods involve high temperature melting, the CNCs are unable to withstand the processing conditions [5,6].

Typically, CNC polymer nanocomposites are restricted to processing methods such as solution casting. While this process is great for preserving the dispersive state of the CNCs in solution, it is not industrially viable [6,11]. Moreover, large-scale solvent use is not economically viable and it has been proclaimed that ideal green manufacturing is entirely solvent-free due to growing concern of high production of industrial chemical waste [12]. To this end, conventional methods like melt extrusion have been explored for processing these nanocellulose based polymer composites, specifically incorporating CNCs into poly (lactic acid) PLA and polyethylene (PE) [13–16]. Melt compounding and injection molding are two of the most commonly used industrial processing methods for thermoplastics and being able to incorporate CNCs into the system could be revolutionary for the industry [5]. However, in all these works, some additional processing aids or surface functionalization of CNCs were used in an attempt to overcome the challenges of thermal stability and aggregation of CNCs. A variety of functionalization of the surface of CNCs have been studied indicating the hindrance of their inherent nature to aggregate, and phosphating the CNCs has even restored their thermal stability unlike sulfonation [5,7,10]. While this method has shown to be successful when the composites were melt processed, it is time-consuming and at times complicated and expensive to functionalize the CNCs that make it unsuitable for industrial applications. Therefore, these conventional processing techniques for the preparation of CNCs reinforced polymer nanocomposites have been disregarded due to their inherent incompatibility and lack of thermal stability and few solutions have been proposed to tackle this challenge [2].

Melt compounding using phosphated-CNCs and PA12 has also been shown with relative success [10]. Additionally, the successful melt compounding of solution cast polyvinyl acetate (PVAc)/CNCs nanocomposites with minimal to no mechanical degradation by using low shear conditions was demonstrated indicating the potential importance of pre-mixing [5,17]. Furthermore, coating of the CNCs with polyethylene oxide (PEO), polyamide 6 (PA6), or polystyrene (PS) by freeze-drying or precipitating in water prior to melt processing like extrusion was conducted with encouraging results showing improvement in dispersibility and thermal stability [2,18,19].

Furthermore, Peng et al. developed CNC reinforced PA 11 through solution casting followed by compression molding resulting in a reduction of toughness, and improved mechanical properties only with dodecanoic acid surface modified CNCs [20]. Herein, we propose an industrially scalable method of preparing high performance PA 11/cellulose nanocomposites, furthering the sustainability initiative, with improved mechanical properties for melt processing at elevated temperatures. In this study, simpler preprocessing/premixing methods such as planetary ball milling and melt-compounding (roller blade mixing) without the addition of processing aids or additional surface functionalization of CNCs are explored to obtain nanocomposites suitable for industrial melt processing, like injection molding, at elevated temperatures while retaining the thermal and mechanical integrity of the material.

2. Materials and methods

The PA 11 used was obtained originally in a pellet form from Arkema Rilsan®. Cellulose nanocrystals (CNCs) materials were obtained from two sources, 1). as freeze-dried product from Forest Products Lab (FPL) (sulfuric acid hydrolysis, from wood pulp; 0.94 wt% sulfur content on dry CNCs), and 2). as spray dried product from CelluForce Inc. (sulfuric acid hydrolysis, from wood pulp; 0.86–0.89 wt% sulfur content on dry CNCs). For the rest of this paper, the FPL CNCs will be denoted as *FPL-CNCs*, while the CelluForce CNCs will be denoted as *CF-CNCs*.

2.1. Processing of PA 11/CNC nanocomposites

2.1.1. Cryo-milling and planetary ball milling

In order to mill CNCs into the PA 11 successfully, the pellets had to be milled into powders first using a cyromill. For this instrument, a considerable amount of the milling vial had to be free volume to allow space for collisions. Planetary ball milling was utilized to embed the CNCs within the PA 11 particles. This process uses ball bearing collisions to mechanically weld together two materials in the solid state without solvents. This is a typically low shear environment compared to other milling techniques like high energy ball milling (HBM). The charge ratio of 15 was used with a milling time of 6 h. Additionally, the ball bearing size used was ¼" (6.35 mm).

2.1.2. Melt compounding (roller-blade mixing)

A 10 wt% PA 11/CNC composite was prepared by melt compounding using a roller blade type mixer, (C.W Brabender® Mixer). Direct melt mixing allowed bypassing the use of a solvent system and increased the potential scalability of the procedure. To effectively melt and mix the polymer pellets, the temperature was set to 190 °C with a rotor speed of 70 rpm. The PA 11 was added to the instrument and allowed to mix for 6 min prior to adding the CNCs. After the addition of CNCs, the mixing was continued for four more minutes. The mixed material was then removed from the mixer and allowed to cool to room temperature.

2.2. Testing of PA 11/CNC nanocomposites

2.2.1. Compression molding

The composite material obtained from the compounding and milling was compression molded using a Carver® press, at 190 °C under a pressure of 3 metric tons for 5 min. Spacers were placed to control the thickness, producing films of approximately 150 μm. The compounded films were transparent with no optical signs of aggregation by the CNCs. However, some aggregation of CNCs was observed in the milled films.

2.2.2. Thermal properties

Thermogravimetric analysis (TGA) was performed with a TA Q500. The temperature ranged from 25 °C to 600 °C with a heating rate of 10 °C/min. The tests were carried under nitrogen with a flow rate of 40 mL/min. All results were analyzed using the Universal Analysis software.

Additionally, Differential Scanning Calorimetry (DSC) was carried out with a TA Q800. The samples ranging 5–9 mg were measured and placed in aluminum pans. The samples underwent a heat-cool-heat cycle under nitrogen atmosphere with the temperature ranging from −30 °C to 230 °C. The heating rate was 10 °C/min, while the cooling rate was 5 °C/min. The degree of crystallinity was then calculated for the samples

using Equation (1), where ΔH_f is the experimental heat of fusion of the sample, w is the weight fraction of the PA 11 in the sample, and ΔH_o is the theoretical heat of fusion of 100% crystalline PA 11, which is 226.4 J/g [21]. Additionally, with use of the TA Universal Analysis software, the inflection point glass transition temperature, T_g, values are reported. A study of cooling rate dependence was also done on the neat PA 11 and milled composite samples at rates of 5, 10, 20, and 30 °C/min.

$$X_c(\%) = \frac{\Delta H_f}{w^* \Delta H_o} * 100 \quad (1)$$

Fast Scanning Calorimetry (FSC) was used to analyze the nucleating effect of the CNCs at process-relevant cooling rates and temperatures. This analysis was performed using a Flash DSC 1 device from Mettler-Toledo cooled with a Huber TC100 intracooler. The sensor/sample environment was purged with nitrogen gas using a flow rate of 60 mL/min to prevent sample degradation. According to the recommendation of the instrument provider, the FSC sensors were conditioned and temperature-corrected before loading a sample. Isothermal experiments were carried out between 50 and 150 °C in order to capture a wide range of crystallization data between T_g and T_m. A diagram of the isothermal experiments performed in FSC is presented in Fig. 1. In this experiment, the sample was heated to 220 °C to the molten state. It was then quenched at 2000 K/s to the target isothermal crystallization temperature, where it was held for 3 s. The material was then quenched to −60 °C. A heating segment of 500 K/s was used to take the sample back to the melt state, where it was then cycled through a similar set of steps until all isothermal temperatures were sampled.

FSC experiments were also carried out under non-isothermal cooling conditions to see the nucleating effect of the CNCs at process-relevant cooling rates. A diagram of this method is displayed in Fig. 2. In this method, the sample was taken to the melt at 220 °C. It was then cooled at a specific rate, ranging from 0.1 to 4000 K/s to −60 °C. It was then heated at 500 K/s back to the maximum temperature of 220 °C. This process was repeated for each cooling rate so that the full spectrum of cooling rates could be analyzed in a specific sample.

2.2.3. Water absorption studies

These studies were carried out with periodic mass measurements of melt-pressed compounded and milled films submerged in water over 24 h. Three rectangles of 15 × 5 mm were cut from all 6 different sample films and weighed before placing in diH_2O at room temperature. The films were removed from the water and patted down with Kimwipes® prior to weighing. Mass measurements were recorded at 0 h, 0.5 h, 1 h, 3 h, 6 h, 12 h, 18 h, and 24 h. The percent change was calculated using

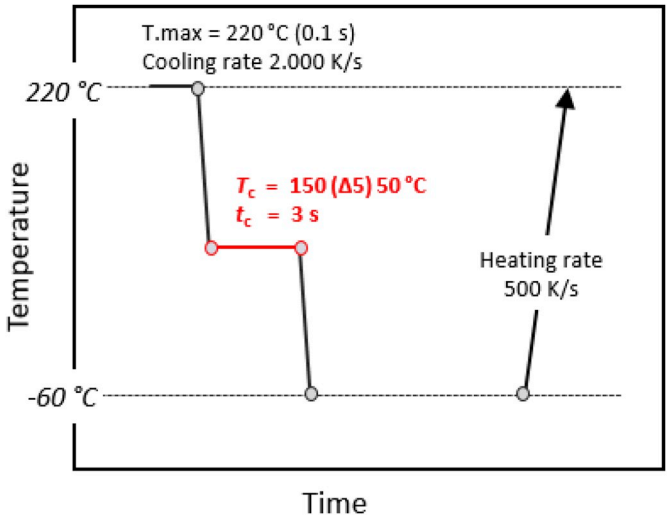

Fig. 1. FSC method for isothermal crystallization.

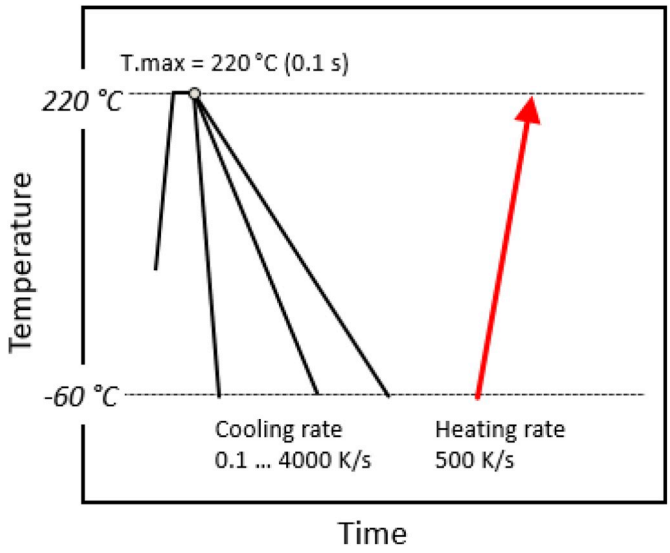

Fig. 2. FSC method for non-isothermal crystallization.

Equation (2), and triplicates of samples were used to obtain statistical significance of data.

$$\frac{(W_{wet} - W_{dry})}{W_{dry}} \times 100 \quad (2)$$

2.2.4. Conductometric Titration

$$\frac{mmol\ SO^{4-}}{kg\ cellulose} = \frac{C_{NaOH} * V_{NaOH}}{W_{CNC}} * 10^6 \quad (3)$$

To determine the surface charge density of the CNCs, conductometric titrations were carried out. CNCs were dispersed in a diH_2O, along with 0.02 M HCl (Sigma Aldrich) and 0.02 M NaCl (Sigma Aldrich). The dispersion was titrated with 0.5 M of NaOH (Sigma Aldrich). Titration conductivity values were determined through plotting against volume of NaOH added.

Analyses were performed in triplicates and equivalence points were obtained from the intersection of the least squares regression lines fit to the data points making up the conductometric titration curve. Equation (3) was used to calculate the surface charge density of the CNCs [7,22].

2.2.5. Mechanical characterization

PA 11/CNC composite materials were tested for their viscoelastic properties with a dynamic mechanical analysis (DMA) using a TA Instruments Model Q800. The samples were cut into rectangular strips and tests were conducted using the tension geometry using a temperature sweep method. The temperature range was set to be from 0 °C to 220 °C, a fixed frequency of 1 Hz, a strain amplitude of 15 μm, and a heating rate of 10 °C/min.

Additionally, tensile testing for the composites was conducted using a 500 N Instron® machine on the melt pressed compounded and milled films. Tests were carried out at room temperature at a strain rate of 5 mm min^{-1} and a gauge distance of 10 mm. Dog-bone shaped films were cut out of the melt pressed films for testing. Repeated trials were conducted to determine statistical significance.

Lastly, the rheology of the materials was studied using an Instron® CEAST SmartRHEO (SR20) capillary rheometer system. The temperature was set to 210 °C and ten logarithmically spaced shear rates between 100 and 1000 s^{-1} were measured. The capillary die had a diameter of 1 mm and L/D of 30, used to minimize the impact of die entry effects. For both compounded and milled composites, samples were poured into the capillary barrel and manually packed to remove any air bubbles. A compacting force of 1000 N was then applied during a

2 min preheat cycle to ensure homogenous packing and uniform heating.

3. Results and discussion

PA 11/CNC nanocomposites were prepared using S–CNCs obtained from two commercial sources, both derived from wood using sulfuric acid hydrolysis. Samples were either made by milling or compounding. The milling process involved first cyromilling the PA 11 pellets into powder particles, followed by planetary ball milling the CNCs into the PA 11. For the compounding, roller blade mixing was used to mix the CNCs into the PA 11 melt. Schematics of these process are shown in Fig. 3, along with the homogeneous films obtained by compression molding the nanocomposite material obtained from these processes. The films show that no aggregation of CNCs is observable and that the compounding resulted in some color change due to the temperature component of the processing method. The discoloration of the composite films is common for CNC reinforced materials due to the onset of thermal degradation. The negatively charged sulfate half-ester groups on the CNC surface catalyze the degradation of cellulose, especially at higher temperatures [7]. However, previous work from our group has shown that this does not begin to affect the mechanical integrity of the material until browning of the material is observed [10,23].

All samples were made with a CNC content of 10 w/w%. The loading % was kept constant in this study at 10 w/w% based on previous research indicating higher CNC content lead to excess CNC–CNC interactions resulting in poor reinforcement and embrittlement of the overall material [10,24]. While lower amounts of CNCs may increase the nucleation efficiency to further reinforce the polymer, the reduction of CNCs will also aid in ease of processing due to their thermal stability limitations. Herein, we wanted to show the success of processing with relatively high amount of CNCs to further highlight the influence of the pre-mixing methods. Compositional analysis produced a TGA thermogram showing successful integration of 10 wt% CNCs within the PA 11 using both the milling and compounding premixing methods. Furthermore, the TGA was useful in characterizing the thermal stability of the nanocomposites in comparison to the neat polymer. The thermograms explicated the range for processing temperatures for the nanocomposites as well.

Additionally, DSC characterization elucidated the melt and crystallization behavior of the samples as shown in Table 1. The overall crystallinity of the PA11 in the nanocomposites compared to the neat PA 11 samples does increase, especially seen in the FPL-CNC milled sample and both the compounded samples. Furthermore, it is apparent that the processing does reduce crystallinity of the PA 11, with the compounding having a larger effect. Compared to the neat PA 11 as received, there is a slight decrease in the melt temperature, Tm, for most of the nanocomposites, and little change to the crystallization temperature, T_c. This could be due to the loading amount of the CNCs. The addition of CNCs, if well dispersed within the polymer matrix could decrease the overall crystallite size, thereby increasing the amorphous regions. This is especially seen with the milled CF-CNC milled sample which displays a lower percent crystallinity. It is possible that the CNCs in this sample are better dispersed in comparison to the other composites.

Table 1
Summary of DSC data of neat PA 11 as received compared to processed Neat PA 11 and the processed nanocomposites.

Sample	T_g (°C)	T_m (°C)	ΔH_m (J/g)	T_c (°C)	X_c (%)
Neat PA 11	43.9	190.4	51.7	165.8	22.8
Neat PA 11 Mi	42.5	188.9	46.7	166.2	20.6
Neat PA 11 Co	44.1	189.0	38.6	166.1	17.0
PA 11-FPL-CNC Mi	42.7	188.5	47.8	166.2	23.5
PA 11-FPL-CNC Co	42.7	189.5	44.5	166.1	21.8
PA 11-CF-CNC Mi	47.7	190.6	35.6	167.1	17.5
PA 11-CF-CNC Co	42.8	189.5	50.4	166.4	24.8

Fig. 3. Schematic of pre-mixing processes of milling (Mi) and compounding (Co), specifically cryo-milling to reduce pellets down to micron sized powder particles followed by planetary ball milling to incorporate the CNCs in the polymer particles; and roller blade mixing to develop homogeneously dispersed nanocellulose/PA 11 composites.

The subdued increase in % crystallinity as reported in Table 1, however, is likely an artifact of the slow cooling rate at 5 °C/min as Fig. 4 clearly shows the impact of CNCs nucleating the PA 11 at higher cooling rates.

Isothermal data traces from FSC testing are displayed in Fig. 5. From these curves, the peak of the exothermal event was used to understand the time dependence of crystallization at each temperature. A data set such as the one displayed in this figure was also analyzed for the nucleated PA 11 materials.

All of this data was compiled, which is presented in Fig. 6. This data shows a bi-modal temperature dependence on crystallization, which is common for polyamide systems [25–27]. It has been shown specifically for PA 11 that the high temperature regime is due to heterogeneous nucleation, producing δ-crystals of spherulitic morphology. The low temperature regime has been shown to result from homogeneous nucleation, producing the δ′-mesophase [25]. The nucleating behavior, as displayed by the decrease in peak-time of crystallization in the heterogeneous regime, has recently been established in systems such as nucleated polypropylene [28]. Looking to the nucleating efficiency of the two grades of CNCs studied in this work, the isothermal crystallization behavior shows that PA 11-FPL-CNC has slightly better nucleating effects than PA 11-CF-CNC, as indicated by a lower crystallization time.

A non-isothermal analysis was used to analyze the nucleating efficiency of the material at rates that are applicable to common plastics manufacturing applications. It has been found that typical cooling rates experienced in injection molding can reach up to 600 K/s where the molten polymer meets the cold steel mold wall [29]. For this reason, the high cooling rates obtainable by FSC is necessary to assess nucleation efficiency at process-relevant conditions. In this analysis, cooling rates as low as 0.1 K/s (6 K/min) and as high as 4000 K/s were assessed. In order to analyze the crystallization that occurred on cooling, the subsequent heating trace was analyzed. The plot below shows the melting enthalpy after each specified cooling rate. Since even FSC heating rates cannot outpace cold crystallization in PA 11, if cold crystallization occurred, it was subtracted from the melting enthalpy. Fig. 7 shows the resulting enthalpy as a function of cooling rate. It is apparent that the CNCs are able to nucleate the PA 11 system because crystallization is able to initiate at a higher rate. As displayed in the figure, crystallization is completely suppressed at cooling rates of 300 K/s and greater, but when the system is nucleated, the critical cooling rate required to suppress crystallization is increased to 500 K/s.

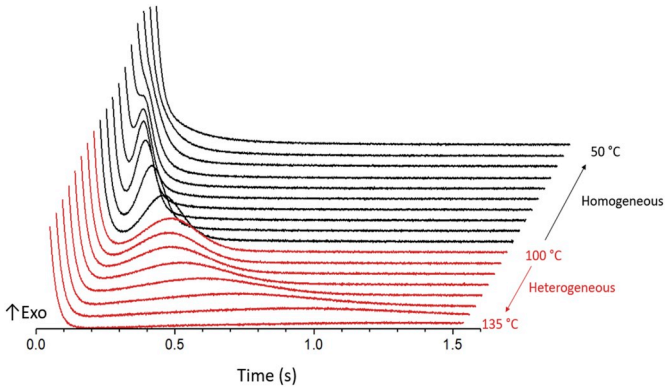

Fig. 5. Set of FSC curves, heat-flow rate as a function of time, obtained during isothermal crystallization of PA 11 at temperatures between 50 °C (back) and 135 °C (front), with each curve indicating the isothermal trace with a change in temperature of 5 °C.

Additionally, due to the hydrophilic nature of CNCs, a water uptake study was conducted gravimetrically over a 24 h period, with mass measurements taken periodically at 0 h, 30 min, 1 h, 3 h, 6 h, 12 h, 18 h, and 24 h to test the effects of water on the nanocomposites and therefore their mechanical integrity over time. The water absorption study indicated the lack of significant water uptake. Any increase in water absorption was within error and deviance of the instrument. The polymer acting as a protective layer around the CNCs because of the pre-mixing could be inhibiting the CNCs from the water uptake. Although the amide groups on polyamides make them hydrophilic, compared to shorter chained polyamides, PA 11 has less polarity. Additionally, this behavior can be ascribed to the strong hydrogen bonding between the CNCs and the polymer matrix as well as to the CNC–CNC interactions which are competing with water [2].

Higher CNC content can lead to excess CNC–CNC interactions resulting in poor reinforcement and embrittlement of the overall material. The hydroxyl groups on the CNCs result in strong hydrogen bonding between them thereby developing a percolating network within the polymer matrix. However, keeping within the limit of the percolation threshold that is dependent on the aspect ratio of the CNCs is essential to obtain reinforcement of the polymer because aggregation of the CNCs could negate the nanoscale characteristic and thereby potential for

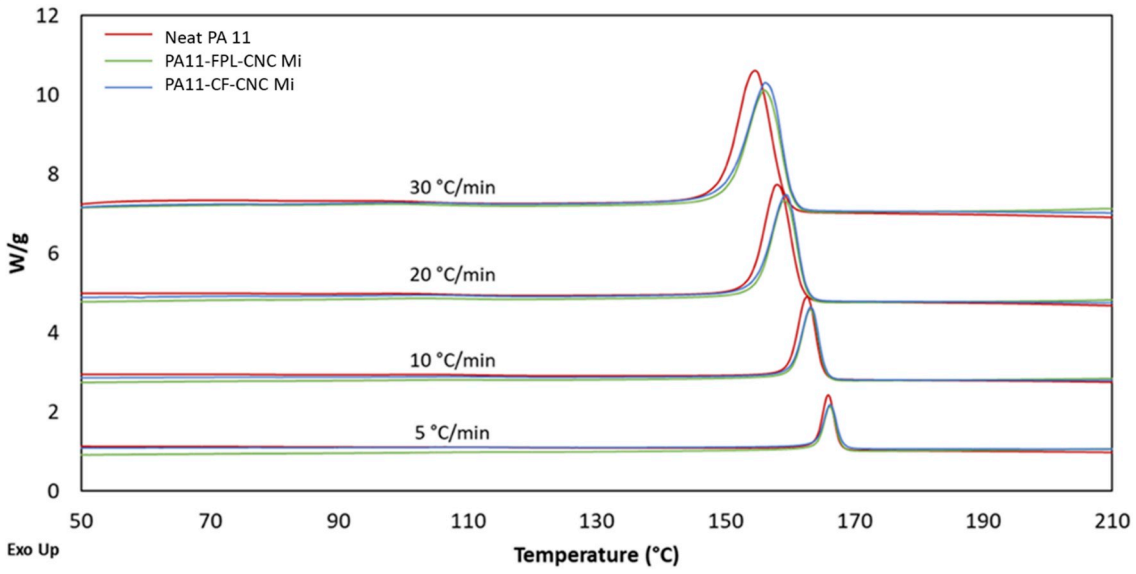

Fig. 4. DSC of PA 11/CNC milled composites compared to neat PA 11 showing the relationship between cooling rate and respective crystallization.

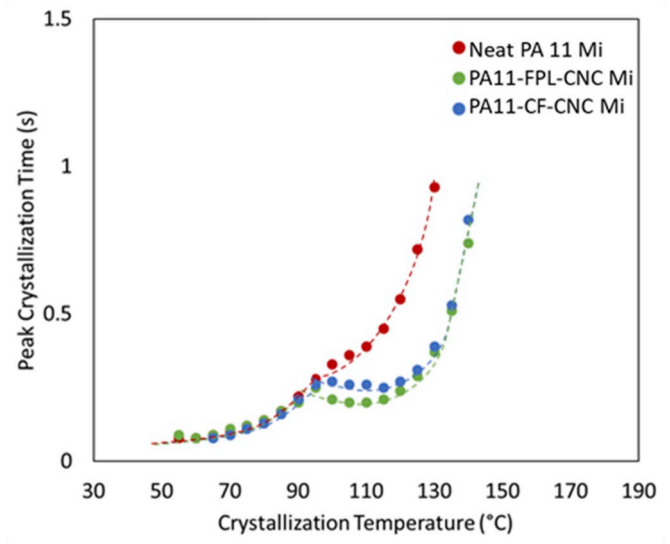

Fig. 6. Peak time of isothermal crystallization of neat PA 11 and nucleated PA 11 with FPL-CNCs and CF-CNCs. The dashed lines are a guide for the eyes.

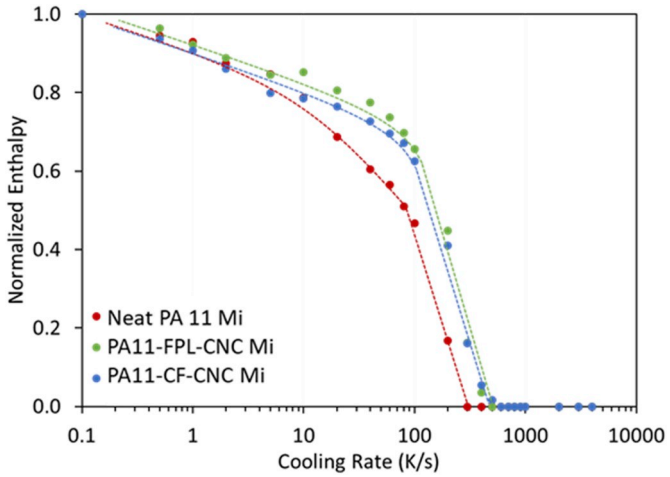

Fig. 7. Normalized relative crystallinity as a function of cooling rate. To normalize, the enthalpy obtained at 0.1 K/s was used as the maximum relative crystallinity. The dashed lines are a guide for the eyes.

mechanical reinforcement [3,30]. Therefore, homogeneous dispersion of the CNCs and loading amount are key variables in obtaining optimal mechanical properties in the nanocomposite. The DMA indicated significant reinforcement of the PA 11 with the addition of the CNCs as seen in Fig. 8. Especially at temperatures above the glass transition temperature, T_g, the storage modulus of the composites outperforms the neat PA 11 samples in both the milled and compounded processed samples. Table 2 summarizes the mechanical properties of the nanocomposites based on processing method and type of CNCs. While looking at the tensile testing data, it appears that the composite integrated with the CF-CNCs are tough with a % elongation break almost matching that of the PA 11 while exhibiting a higher elastic modulus especially for the samples processed through milling. With respect to the DSC data, the CF-CNCs milled samples did display less crystallinity, perhaps due to a reduction in crystallite size and an increase in amorphous regions, resulting in an increase in ductile behavior and therefore overall toughness of the material.

This is unlike the brittle behavior observed for the composite with the FPL-CNCs. It should also be noted that the ultimate tensile strength of the composites for both types of CNCs and with regard to both processing methods is more than 2x higher for the milled samples and 4x higher for the compounded samples than the ultimate tensile strength of the neat PA 11. It is apparent that processing of the neat PA 11 reduces the mechanical properties compared to the non-processed PA 11. It should also be noted that the milling resulted in higher mechanical properties compared to the compounded which can be attributed to the compromised thermal stability of the CNCs at the higher temperature required for compounding. It is possible that the dispersion obtained with the CF-CNC compounded samples is poorer, and the higher surface charge of the CF-CNC perhaps also results in some thermal degradation and overall lower mechanical properties compared to the compounded FPL-CNC. With both processing methods, the toughness shown from the CF-CNC composite samples could be attributed to the surface charges on the CNCs resulting in more of a repulsion with respect to CNC–CNC interactions as corroborated by the conductometric titration. This phenomenon drives better interaction between the CNCs and the polymer itself allowing for enhanced reinforcement. Overall, this data indicates that an increase in mechanical properties is largely due to the addition of CNCs and the interaction of them with the PA 11.

The mechanical behavior observed here of these S–CNC based composites are lower than that of phosphated CNCs (P–CNC)/PA-12 composites as shown in Nicharat et al. perhaps due to the higher thermal stability of P–CNCs [10]. Moreover, the reinforcement observed of PA 11 in this study indicates that the processing methods did not compromise the crystallinity significantly, which can be ascribed to the low shear conditions of the pre-mixing methods. Overall, the compounded samples seemed to have both lower stiffness and ultimate tensile strength, compared to the milled samples, indicating that perhaps the processing technique has an impact on the crystallinity. However, more variability was seen in the milled samples, indicating homogeneity is better achieved through compounding. With this data, it can be concluded that the successful integration of CNCs to produce a homogeneous sample can result in significant enhancement of mechanical properties of PA 11.

The rheology of these composites was characterized to determine melt flow properties, specifically the shear rate dependence of their viscosity. This study was conducted in order to confirm the processability of these nanocomposites through characterization at process-relevant shear rates. Testing via capillary rheometry allowed characterization in a system most closely matching that of injection molding due to the presence of hydrostatic pressure [31,32]. The addition of CNCs resulted in slightly higher viscosities compared to the neat PA 11 for the samples reinforced with FPL-CNCs and the compounded CF-CNC samples as shown in Fig. 9. All materials showed similar shear thinning behavior with all but the compounded CF-CNC sample showing slightly higher viscosities at all shear rates. Typically, the addition of fillers in a polymer matrix causes the viscosity of the material to increase due to the hydrodynamic effect and the filler network. At low CNC concentrations, the CNCs are predominantly free particles, therefore having higher mobility compared to high concentrations. At high CNC concentrations, the network structure obtained through percolation of CNCs prevents mobility of the particles resulting in high shear stresses. This behavior can be attributed to the hydrodynamic effect where the inextensibility of the CNCs results in transferring of stresses onto the polymer chains [33,34]. The percolation model can be understood in conjunction with lag-shear behavior that describes the load transfer between the networked CNCs and the polymer chains [35]. However, in these composites, the viscosity remained relatively similar to the neat PA 11, perhaps due to ideal loading amounts and aspect ratio of the CNCs. Overall, this data indicated desirable behavior for injection molding. Likely due to optimal loading and the aspect ratio of the CNCs, the viscosity did not increase much, indicating good dispersion, and suggesting the presence of a percolating network. The CF-CNC milled sample does display slightly lower viscosity especially around 100 1/s shear rates, which aligns with the thermal and mechanical characterization shown earlier due to its reduced overall % crystallinity.

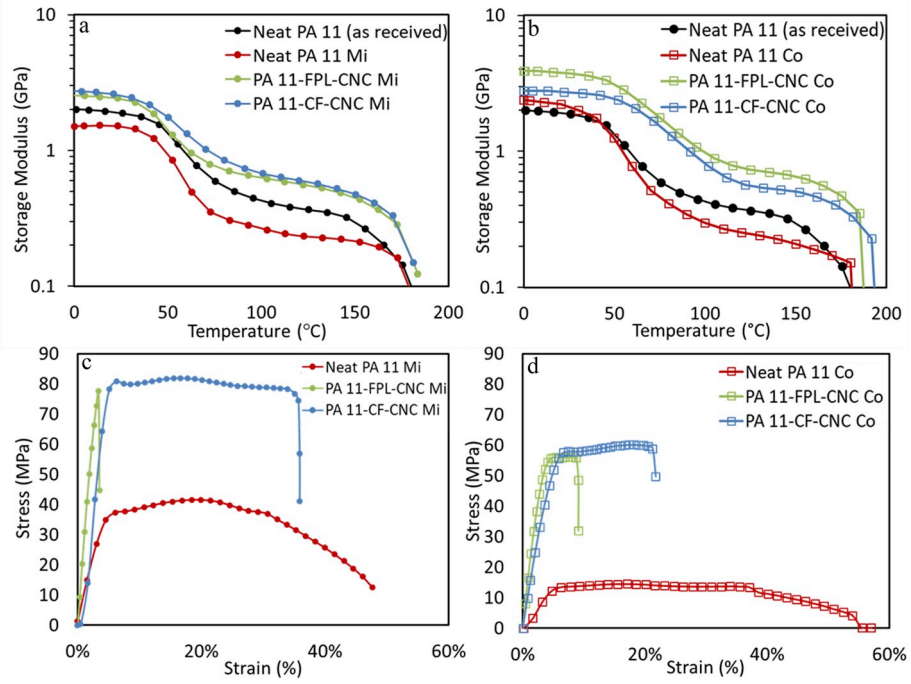

Fig. 8. Dynamic mechanical analysis (DMA) of samples prepared using a). milling, and b). compounding, Stress/Strain curves of samples prepared through c). milling and d). compounding.

Table 2
Tensile Properties of PA 11/CNC Nanocomposites for Samples Processed through both milling and compounding with both FPL-CNCs and CF-CNCs

	Young's Modulus (MPa)		Ultimate Tensile Strength (GPa)		% Elongation at Break	
	Milled	Compounded	Milled	Compounded	Milled	Compounded
Neat PA 11	800 ± 180	330 ± 80	42 ± 7	15 ± 5	49% ± .5	55.1% ± 3.7
FPL-CNC	2250 ± 300	1690 ± 103	78 ± 6	56 ± 2	4.2% ± .8	9.1% ± .4
CF-CNC	2310 ± 145	1240 ± 58	82 ± 10	60 ± 4	36% ± 1.1	21.8% ± .3

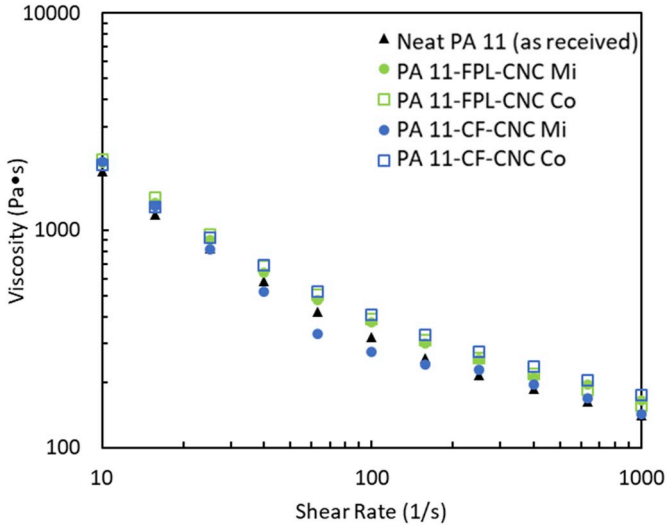

Fig. 9. Rheological Behavior of milled and compounded 10 wt% CNCs in PA 11 composites compared to neat PA 11.

Additionally, all samples displayed non-Newtonian behavior indicated by the decreasing viscosity with increasing shear rates. Typically, high CNC loading and poor dispersion of the CNCs within the polymer matrix can lead to jamming effects indicated by the switching from shear thinning to shear thickening behavior at higher shear rates. However, with these nanocomposites, the rheological behavior further corroborates the success of pre-mixing, the optimal CNC content, and good dispersion of CNCs within the polymer matrix.

The dispersibility of CNCs in a polymer matrix is strongly dependent on the electrostatic repulsion between the nanocrystals [22,36,37]. The surface charge density of the CNCs that governs the electrostatic interaction can be measured by conductometric titration. Essentially, the conductivity of the CNCs decreases as acid sulfate esters are deprotonated and replaced by sodium cations as NaOH is added and it increases once the volume of added NaOH exceeds the amount required for neutralization [22]. Conductometric titration indicated that the FPL-CNCs have a charge density of 306 mmol of functional group/kg CNC ± 20, and CF-CNCs have a charge density of 509 mmol of functional group/kg NC ± 35. The higher charge density of the CF-CNCs results in better dispersion of the CNCs in the polymer matrix compared to the FPL-CNCs because of a higher amount of electrostatic repulsion between the CNCs. Typically, the higher frequency of amide groups ensuing from the use of shorter chained polyamides like PA 6 and PA 66 result in more hydrophilicity and therefore better interaction with CNCs. The longer chain of PA 11 and therefore lower frequency of amide groups certainly poses a challenge and the high surface charge density of the CNCs is being taken advantage of to improve interaction with the polymer matrix as a direct result of electrostatic repulsion [10].

4. Conclusion

With PA 11 being such a hot commodity in the aerospace and automobile industries due to their eco-friendly nature and attractive

materials properties, there is a lot of attention being placed on enhancement of mechanical properties using nanofillers. CNCs therefore are an obvious choice due to their concurrent eco-friendly nature as well as their high crystallinity, aspect ratio, and reinforcement capabilities. The successful incorporation of CNCs in PA 11 results in an essentially carbon-neutral, recyclable, and sustainable material. However, unless polymer/CNC nanocomposites can be produced at an industry scale, the use of alternative fillers like carbon nanotubes and glass fibers will continue to be the industry standard despite their lack of being bio-based or providing comparable mechanical enhancement. Through this study, milling and compounding have both proven to be viable pre-mixing methods to obtain melt processable polymer/CNC nanocomposites. Moving forward, injection molding of dog bones and mechanically characterization of the 10 wt% FPL-CNCs and CF-CNCs milled and compounded composite material will further aid in optimizing processing conditions with respect to time and temperature. Minimizing exposure at high temperatures is critical to obtaining injection molded parts that retain their integrity by inhibiting thermal degradation of the CNCs. This is true for other melt processing techniques as well and use of these composite materials will require process optimization. Ultimately, this study provides a promising outlook for sustainable, industrial-scale manufacturing of high performance, nanocellulose reinforced polymeric composites.

Acknowledgements

The authors acknowledge the financial support received from the Department of Energy SBIR grant (DE-SC0018051) and our colleagues at Innovatech, Inc., Raghuram Dhumpa and Kris Kelly. Additionally, supported by the National Science Foundation under Grant CMMI-1653629. The authors acknowledge and thank Alex Aning and Jonathan Angle for access to and assistance with all milling equipment, Justin Barone – Renewable Materials Laboratory for access to their roller blade mixer, (C.W Brabender® Mixer), Michael Bortner – Polymer Composite and Materials Laboratory in the Advanced Manufacturing Group for access to and guidance with the Instron® CEAST SmartRHEO (SR20) capillary rheometer, and Chip Frazier – Sustainable Biomaterials for access to the auto-titrator.

References

[1] Xiaoli Y, Krifa M, Koo JH. Flame-retardant polyamide 6/carbon nanotube nanofibers: processing and characterization. J Eng Fabr Fibers (JEFF) 2015;10(3):1–11.
[2] Marcos M, Nadia EK, Alain D. Cellulose nanocrystals and related nanocomposites: review of some properties and challenges. J Polym Sci, Part B: Polym Phys 2014;52(12):791–806.
[3] Dufresne A. Nanocellulose: a new ageless bionanomaterial. Mater Today Off 2013;16(6):220–7.
[4] Yeh WY, Young RJ. Molecular deformation processes in aromatic high modulus polymer fibres. Polymer 1999;40(4):857–70.
[5] Janak S, Sandeep K, Christoph W, Johan FE. Influence of processing conditions on properties of poly (vinyl acetate)/cellulose nanocrystal nanocomposites. Macromol Mater Eng 2015;300(5):562–71.
[6] Miao C, Hamad WY. Cellulose reinforced polymer composites and nanocomposites: a critical review. Cellulose 2013;20(5):2221–62.
[7] Camarero Espinosa S, Kuhnt T, Foster EJ, Weder C. Isolation of thermally stable cellulose nanocrystals by phosphoric acid hydrolysis. Biomacromolecules 2013;14(4):1223–30.
[8] Habibi Y, Lucia LA, Rojas OJ. Cellulose nanocrystals: chemistry, self-assembly, and applications. Chem Rev 2010;110(6):3479–500.
[9] George J, Sabapathi SN. Cellulose nanocrystals: synthesis, functional properties, and applications. Nanotechnol Sci Appl 2015;8:45–54.
[10] Nicharat A, Sapkota J, Weder C, Foster EJ. Melt processing of polyamide 12 and cellulose nanocrystals nanocomposites. J Appl Polym Sci 2015;132(45) [n/a-n/a].
[11] Hamad WY. Cellulose nanocrystals: properties, production and applications. Wiley; 2017.
[12] Long TE, Hunt MO. Solvent-free polymerizations and processes: recent trends in the minimization of conventional organic solvents. In: Solvent-free polymerizations and processes, vol 713. American Chemical Society; 1999. p. 1–5.
[13] Junior de Menezes A, Siqueira G, Curvelo AAS, Dufresne A. Extrusion and characterization of functionalized cellulose whiskers reinforced polyethylene nanocomposites. Polymer 2009;50(19):4552–63.
[14] Oksman K, Mathew AP, Bondeson D, Kvien I. Manufacturing process of cellulose whiskers/polylactic acid nanocomposites. Compos Sci Technol 2006;66(15):2776–84.
[15] Raquez JM, Murena Y, Goffin AL, Habibi Y, Ruelle B, DeBuyl F, Dubois P. Surface-modification of cellulose nanowhiskers and their use as nanoreinforcers into polylactide: a sustainably-integrated approach. Compos Sci Technol 2012;72(5):544–9.
[16] Bondeson D, Oksman K. Dispersion and characteristics of surfactant modified cellulose whiskers nanocomposites. Compos Interfac 2007;14(7–9):617–30.
[17] Nicharat A, Sapkota J, Foster EJ. Pre-mixing and masterbatch approaches for reinforcing poly(vinyl acetate) with cellulose based fillers. Ind Crops Prod 2016;93:244–50.
[18] Lin N, Dufresne A. Physical and/or chemical compatibilization of extruded cellulose nanocrystal reinforced polystyrene nanocomposites. Macromolecules 2013;46(14):5570–83.
[19] Ben Azouz K, Ramires EC, Van den Fonteyne W, El Kissi N, Dufresne A. Simple method for the melt extrusion of a cellulose nanocrystal reinforced hydrophobic polymer. ACS Macro Lett 2012;1(1):236–40.
[20] Peng SX, Shrestha S, Youngblood JP. Crystal structure transformation and induction of shear banding in Polyamide 11 by surface modified cellulose nanocrystals. Polymer 2017;114:88–102.
[21] Inoue M. Studies on crystallization of high polymers by differential thermal analysis. J Polym Sci - Part A Gen Pap 1963;1(8):2697–709.
[22] Abitbol T, Kloser E, Gray DG. Estimation of the surface sulfur content of cellulose nanocrystals prepared by sulfuric acid hydrolysis. Cellulose 2013;20(2):785–94.
[23] Sapkota J, Natterodt JC, Shirole A, Foster EJ, Weder C. Fabrication and properties of polyethylene/cellulose nanocrystal composites. Macromol Mater Eng 2017;302(1):1600300.
[24] Sapkota J, Jorfi M, Weder C, Foster EJ. Reinforcing poly(ethylene) with cellulose nanocrystals. Macromol Rapid Commun 2014;35.
[25] Mollova A, Androsch R, Mileva D, Schick C, Benhamida A. Effect of supercooling on crystallization of polyamide 11. Macromolecules 2013;46(3):828–35.
[26] van Drongelen M, Meijer-Vissers T, Cavallo D, Portale G, Poel GV, Androsch R. Microfocus wide-angle X-ray scattering of polymers crystallized in a fast scanning chip calorimeter. Thermochim Acta 2013;563:33–7.
[27] Gohn AM, Rhoades AM, Wonderling N, Tighe T, Androsch R. The effect of supercooling of the melt on the semicrystalline morphology of PA 66. Thermochim Acta 2017;655:313–8.
[28] Schawe JEK, Pötschke P, Alig I. Nucleation efficiency of fillers in polymer crystallization studied by fast scanning calorimetry: carbon nanotubes in polypropylene. Polymer 2017;116:160–72.
[29] Gohn AM, Rhoades AM, Okonski D, Androsch R. Effect of melt-memory on the crystal polymorphism in molded isotactic polypropylene. Macromol Mater Eng 2018;303(8):1800148.
[30] Bras J, Viet D, Bruzzese C, Dufresne A. Correlation between stiffness of sheets prepared from cellulose whiskers and nanoparticles dimensions. Carbohydr Polym 2011;84(1):211–5.
[31] Dealy JM, Wissbrun KF. Role of rheology in injection molding. In: Melt rheology and its role in plastics processing: theory and applications. Boston, MA: Springer US; 1990. p. 491–508.
[32] Guidelines For Rheological Characterization Of Polyamide Melts. Pure Appl Chem 2009;81(2):339–49.
[33] Guth E. Theory of filler reinforcement. J Appl Phys 1945;16(1):20–5.
[34] Cao Y, Zavattieri P, Youngblood J, Moon R, Weiss J. The relationship between cellulose nanocrystal dispersion and strength. Constr Build Mater 2016;119:71–9.
[35] Changsarn S, Mendez JD, Shanmuganathan K, Foster EJ, Weder C, Supaphol P. Biologically inspired hierarchical design of nanocomposites based on poly(ethylene oxide) and cellulose nanofibers. Macromol Rapid Commun 2011;32(17):1367–72.
[36] Beck S, Bouchard J, Berry R. Dispersibility in water of dried nanocrystalline cellulose. Biomacromolecules 2012;13(5):1486–94.
[37] Araki J. Electrostatic or steric? – preparations and characterizations of well-dispersed systems containing rod-like nanowhiskers of crystalline polysaccharides. Soft Matter 2013;9(16):4125–41.